Biomaterials Science

ROYAL SOCIETY OF CHEMISTRY

PAPER

View Article Online
View Journal | View Issue

Cite this: *Biomater. Sci.*, 2023, **11**, 6135

In vivo targeting of a tumor-antigen encoded DNA vaccine to dendritic cells in combination with tumor-selective chemotherapy eradicates established mouse melanoma†‡

Sugata Barui, *§¶[a] Soumen Saha, §‖[a,b] Yakati Venu,**[a,b] Gopi Krishna Moku [a,b,c] and Arabinda Chaudhuri *[a,b,d]

Despite remarkable progress during the past decade, eradication of established tumors by targeted cancer therapy and cancer immunotherapy remains an uphill task. Herein, we report on a combination approach for eradicating established mouse melanoma. Our approach employs the use of tumor selective chemotherapy in combination with *in vivo* dendritic cell (DC) targeted DNA vaccination. Liposomes of a newly synthesized lipopeptide containing a previously reported tumor-targeting CGKRK-ligand covalently grafted in its polar head-group region were used for tumor selective delivery of cancer therapeutics. Liposomally co-loaded STAT3siRNA and WP1066 (a commercially available inhibitor of the JAK2/STAT3 pathway) were used as cancer therapeutics. *In vivo* targeting of a melanoma antigen (MART-1) encoded DNA vaccine (p-CMV-MART1) to dendritic cells was accomplished by complexing it with a previously reported mannose-receptor selective *in vivo* DC-targeting liposome. Liposomes of the CGKRK-lipopeptide containing encapsulated FITC-labeled siRNA, upon intravenous administration in B16F10 melanoma bearing mice, showed remarkably higher accumulation in tumors 24 h post *i.v.* treatment, compared to their degree of accumulation in other body tissues including the lungs, liver, kidneys, spleen and heart. Importantly, the findings in tumor growth inhibition studies revealed that only *in vivo* DC-targeted genetic immunization or only tumor-selective chemotherapy using the presently described systems failed to eradicate the established mouse melanoma. The presently described combination approach is expected to find future applications in combating various malignancies (with well-defined surface antigens).

Received 24th April 2023,
Accepted 22nd July 2023

DOI: 10.1039/d3bm00702b

rsc.li/biomaterials-science

Introduction

In cancer immunotherapy – arguably the most rapidly emerging cancer therapeutic modality – the power of body's immune cells is harnessed to kill cancer cells. Ever since their discovery in 1973,[1] dendritic cells (DCs) have been shown to play a key role in activating our adaptive immune systems in cancer immunotherapy. The distinguishing abilities of DCs in capturing and processing tumor antigens and in presenting the processed antigenic fragments to the T cells in tumor-draining lymph nodes result in the generation of tumor-specific Cytotoxic T Lymphocytes (CTLs) that kill tumor cells.[2–6] DCs are capable not only of presenting extracellular antigen fragments in complexation with the major histocompatibility complex (MHC) class II molecules to CD4+ T helper (TH) cells but also of cross-presenting the antigen fragments on MHC class I molecules to CD8+ T cells.[7] Such cross-presentation capability of DCs is crucial in mounting anti-tumor immune responses.[7] These potent antigen presentation and T cell activation abilities of DCs

[a]*Biomaterials Group, CSIR-Indian Institute of Chemical Technology, Uppal Road, Tarnaka, Hyderabad-500007, Telangana, India.*
E-mail: arabinda.chaudhuri@iiserkol.ac.in, barui.sugata@gmail.com
[b]*Academy of Scientific & Innovative Research (AcSIR), Ghaziabad, Uttar Pradesh-201002, India*
[c]*Department of Physical Sciences, Kakatiya Institute of Technology and Science, Yerragattu Gutta, Warangal 506 015, Telangana, India*
[d]*Department of Chemical Sciences, Indian Institute of Science Education and Research Kolkata, Mohanpur, Nadia-74126, West Bengal, India*

† CSIR-IICT Manuscript No. IICT/Pubs./2023/149.

‡ Electronic supplementary information (ESI) available. See DOI: https://doi.org/10.1039/d3bm00702b

§ These authors contributed equally to this work.

¶ Present address: Enveda Therapeutics India Private Limited, Genome Valley, Hyderabad-500101, Telangana, India.

‖ Present address: Department of Biomedical Engineering, Duke University, Durham, NC 27708-0281, USA.

** Present address: Department of Chemical and Biological Engineering, The University of Alabama, Tuscaloosa, AL 35487, USA.

are finding widespread uses in designing effective anticancer vaccines.[3,8–11]

In clinical studies involving DC-based cancer vaccines, classically autologous monocytes are first isolated from the patient's body using an apheresis technique, and *ex vivo* differentiation of DCs is effected by exposing the isolated DCs to tumor associated/specific antigens (TAAs/TSAs) in the presence of maturation-inducing agents. Such *ex vivo* matured DCs are finally reinfused back into the patient's body.[9,12–15] DNA vaccination (genetic immunization) is another promising therapeutic modality for mounting anti-tumor immune responses in cancer immunotherapy.[16] In this promising therapeutic modality, autologous DCs are first *ex vivo* transfected with the tumor antigen encoded DNA. *Ex vivo* transfected DCs then process the expressed antigenic proteins (using their proteosome complexes) into small peptide fragments and present the resulting antigen fragments in complexation with MHC-I and MHC-II to CD8+ and CD4+ T-lymphocytes, respectively.[17,18] Effective *ex vivo* DC transfection-based DNA vaccinations for mounting immune responses have been accomplished in the past through the use of numerous DNA vaccine carriers including cationic microparticles,[19,20] cationic peptides,[21] cationic liposomes,[22–27] gold nanoparticles,[28] *etc*. More recent studies reported the development of mannose-receptor selective *in vivo* DC-targeting liposomal[29] and gold nanoparticle[30]-based DNA vaccine carriers for inducing effective and lasting anti-tumor immune responses in mice against melanoma under prophylactic settings (*i.e.* in preventive mode).

Although the above-mentioned priorly reported DNA vaccine carriers could protect mice from post-immunization tumor challenge under preventive settings, they failed to eradicate established mouse tumors under therapeutic settings. This is why DC-transfection-based DNA vaccination strategies are now being combined with other effective therapeutic modalities including chemotherapy, radiotherapy, *etc*. in DC-based cancer immunotherapy.[31–37] To this end, we have begun exploring the therapeutic promises of *in vivo* DC-targeted DNA vaccination in combination with tumor-selective chemotherapy for inducing effective anti-tumor immune responses. Using previously designed *in vivo* DC-targeting cationic liposomes prepared from cationic amphiphile containing both transfection-enhancing guanidine functionality and DC-targeting mannose-mimicking shikimoyl functionality[29] and two newly designed BBB-crossing brain-tumor targeting cationic liposomes, we showed that *in vivo* DC-targeted DNA vaccination (containing brain tumor antigen encoded DNA vaccines) in combination with brain-tumor selective chemotherapy remarkably enhanced the overall survivability of mice bearing orthotopically established mouse glioblastoma.[38,39] Although by using such a combination approach in DC-based cancer immunotherapy, we could accomplish 300–500% enhancement of overall survivability of mice bearing orthotopically established brain tumors, we failed to eradicate the established brain tumor.[38,39]

Herein, we report on the first example of applying our above-mentioned unique combination approach[38,39] in DC-based cancer immunotherapy for eradicating established mouse tumors. In this study, for the tumor-selective chemotherapy component in our combination approach, we used liposomes of a new cationic lipopeptide (CLP, Fig. 1) containing a previously reported,[40] and subsequently, widely exploited[41–44] tumor and tumor endothelial cell targeting CGKRK-ligand in its polar head-group region. The liposomes of CLP contained STAT3siRNA (small interfering RNA against signal transducer and activator of transcription 3) encapsulated in its aqueous core and WP1066 (a commercially available hydrophobic JAK (Janus Kinase)/STAT inhibitor) solubilized in its lipid bilayer region. STAT3, aberrantly activated in many cancer cells, causes continuous transcription of cell growth factors and anti-apoptotic molecules, thereby playing a crucial role in maintaining cancer cell growth and survival.[45] However, since STAT3 is a cytoplasmic transcription factor, it is often difficult to target it directly. To this end, JAKs, the upstream activators of STATs, are being used in both preclinical and clinical settings as potential therapeutic targets for decreasing STAT activation in cancer cells.[46] Cytokines and growth factor ligands provide the initial stimulus for activating the JAK/STAT pathway.[47] For instance, binding of cytokines with their corresponding transmembrane receptors leads to multimerization with other subunits and close physical association of receptor-associated JAKs.[48] Thereafter, the receptor-associated JAKs become activated *via* trans-phosphorylation.[48] The phosphorylated (activated) JAKs then phosphorylate the tyrosine residues on the cytoplasmic region of the cytokine receptor to provide docking sites for the Src Homology 2 (SH2) domain of STAT proteins. Binding of STAT proteins to the phosphorylated intracellular domains of the cytokine receptors eventually leads to activated-JAK-catalyzed phosphorylation of the bound STAT proteins.[49] The phosphorylated (activated) STATs become dimerized, and thereafter, the dimerized STATs are translocated into the nucleus to execute their functions as transcription factors, namely, inducing the expression of genes that regulate cellular proliferation, survival, and invasion, as well as the host immune response.[48,50–52]

This is why many small molecule-based JAK inhibitors are finding widespread uses in inhibiting tumor growth. By inhibiting JAKs, they inhibit the activation (phosphorylation) of STAT proteins, and thereby, inhibit the above-mentioned subsequent downstream JAK–STAT signal transduction processes, eventually arresting the proliferation of cancer cells.[46]

Activation of the transcription factor STAT3 produces several immunosuppressive factors such as VEGF, TGFβ, IL-6 and IL-10, which, in turn, negatively affect the functional maturation of DCs.[53,54] More specifically, these immunosuppressive factors inhibit DC maturation by inhibiting expressions of MHC class II, co-stimulatory molecules CD80 and CD86 and immune-stimulating molecules, such as tumor-necrosis factor (TNF) and IL-12.[55] These factors were our rationale for simultaneously targeting both the widely used JAK2 inhibitor WP1066[38,39,46,56–60] and STAT3siRNA using tumor-targeting liposomes of the CGKRK-lipopeptide (CLP, Fig. 1). In the *in vivo* DC-targeted genetic immunization com-

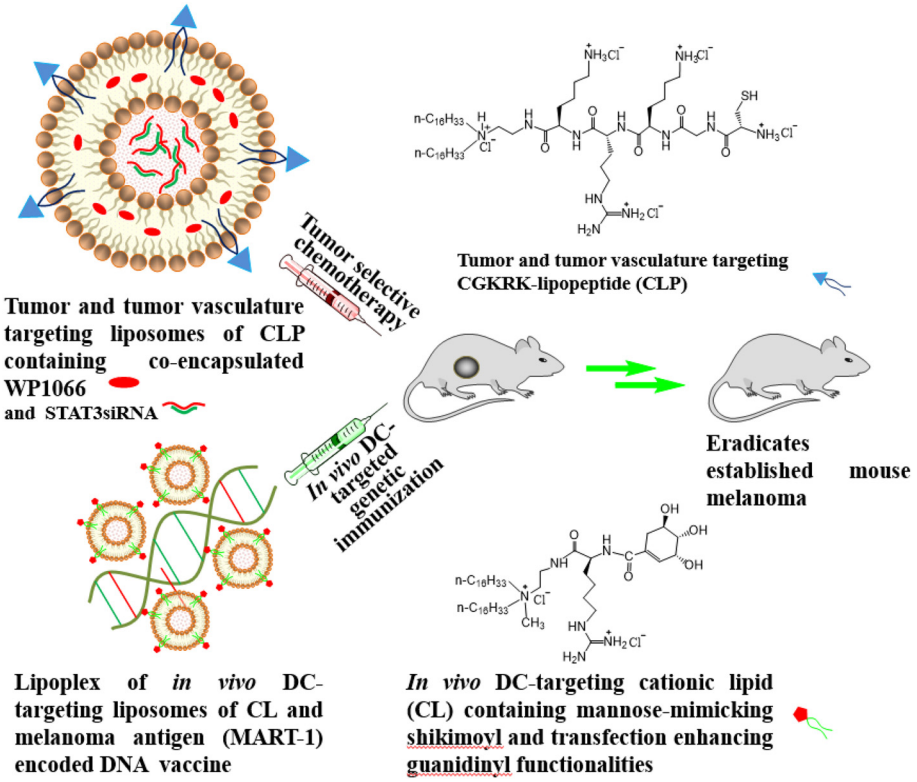

Fig. 1 Cartoon for the presently described combination approach for eradicating the established mouse melanoma tumor. The sizes of the DC-targeting liposomes and the MART-1 encoded DNA vaccine shown in the cartoon are not drawn on the same scale.

ponent of our combination approach, we used a previously reported *in vivo* DC-targeting liposome of a cationic lipid (CL, Fig. 1) containing both transfection-enhancing guanidine and DC-targeting mannose-mimicking shikimoyl head-groups. This *in vivo* DC-targeting cationic liposome was electrostatically complexed with a DNA vaccine p-CMV-MART1 encoding melanoma tumor antigen MART1 (Fig. 1). Selection of p-CMV-MART1 in the present study was based on our prior experience in working with this efficient DNA vaccine.[25–30] Exploiting the abovementioned present systems, herein we show that the combined use of tumor-selective chemotherapy and *in vivo* DC-targeted genetic immunization using tumor antigen encoded DNA vaccines eradicates established mouse melanoma. Such a combination mode may find future uses for the treatment of many cancers where the antigenic markers of the tumor are well characterized.

Experimental

Materials and methods

Reagents, cell lines and animals. Cell culture media, fetal bovine serum, Propidium Iodide (PI), FITC labeled Annexin V, TRIzol reagent, agarose, DOPE, protamine and cholesterol were purchased from Sigma, St Louis, USA. A cell culture lysis reagent, a CTL assay kit and a TUNEL assay kit were purchased from Promega, USA. The VE-cadherin antibody and Texas Red conjugated anti-mouse secondary antibody were purchased from Santa Cruz, USA. Rabbit polyclonal anti-p-STAT3 (Ser 727), rabbit polyclonal anti-STAT3 and rabbit polyclonal anti-β-actin antibodies were purchased from Pierce Biotechnology (Rockford, USA). A goat anti-rabbit alkaline phosphatase conjugated secondary antibody and the BCIP/NBT substrate were purchased from Calbiochem (USA). WP1066, Amicon Ultra centrifugal filter units (10 kD) and a blood vessel staining kit were purchased from Merck-Millipore (USA). Super script III and a first strand cDNA synthesis kit were purchased from Invitrogen Corporation, USA, and PCR Master Mix 2× was purchased from Promega Corporation, USA. STAT3 siRNA, scrambled siRNA and FITC labeled siRNA were purchased from Dharmocon, USA. An IL-4 assay kit and an IFNγ assay kit were purchased from Thermo Fisher Scientific, USA. The CD-31 antibody was purchased from Abcam, USA. Antibiotics were purchased from HiMedia, India. Unless otherwise stated, all reagents were purchased from local commercial suppliers and were used without further purification. B16F10 cells were procured from the National Center for Cell Sciences (NCCS, Pune, India). Cells were cultured in DMEM (Sigma) containing 10% fetal bovine serum (South American Origin, Gibco, USA) and 1% penicillin–streptomycin–kanamycin at 37 °C under a humidified atmosphere of 5% CO_2 in air. Human umbilical vein endothelial cells (HUVECs; Lonza) were cultured in EBM-2 with the recommended supplements. 6–8 weeks old female C57BL/6J mice (each weighing ~20–22 g) were pur-

chased from the National Institute of Nutrition (NIN), Hyderabad, India. All animal procedures were performed in accordance with the Guidelines for Care and Use of Laboratory Animals of CSIR-Indian Institute of Chemical Technology and approved by the Animal Ethics Committee of CSIR-Indian Institute of Chemical Technology.

Synthesis of CGKRK-lipopeptide 1. The Fmoc-strategy-based solid phase peptide synthetic route used for preparing CGKRK-lipopeptide **1** is shown schematically in Fig. 2. 100 mg of H-Lys(BOC)-2-ClTrt resin **1** (N^{ε}-BOC-lysine pre-loaded 2-chloro trityl resin, 0.72–0.77 mmol g^{-1} loading) was first swelled in 10 mL of DMF for 4 h and then coupled with Fmoc-Arg(Pbf)-OH (2 equiv.) using HATU (2 equiv.) and DIPEA (4 equiv.) in DMF at room temperature for 1.5 h to afford intermediate **2**. The resin was then washed with DMF and the Fmoc group was removed with a solution of piperidine : DMF (1 : 4, v/v, 10 mL, 4 min, 2 times) at room temperature. Following the same Fmoc strategy, sequential couplings of Fmoc-Lys(BOC)-OH, Fmoc-Gly-OH and BOC-Cys(Trt)-OH (2 equiv. each) using HATU (2 equiv.) and DIPEA (4 equiv.) in DMF at room temperature for 1.5 h for each amino acid afforded the resin-associated penta-peptide intermediate **3**. The resin-bound intermediate **3** was taken out of the reaction vessel with excess DCM, washed thoroughly with DCM (5 × 10 mL) and dried well. The resulting dried resin bound intermediate was treated with 0.5% TFA in DCM (70 mL) for 2 h at 0 °C to obtain a protected penta-peptide intermediate **4** (0.058 g, 58%). *N*,*N*-Di-*n*-hexadecyl-*N*-2-aminoethylamine (23 mg, 0.046 mmol) was then dissolved in dry DCM (3 mL) and the solution was added to an ice cold reaction mixture (which had been under stirring conditions

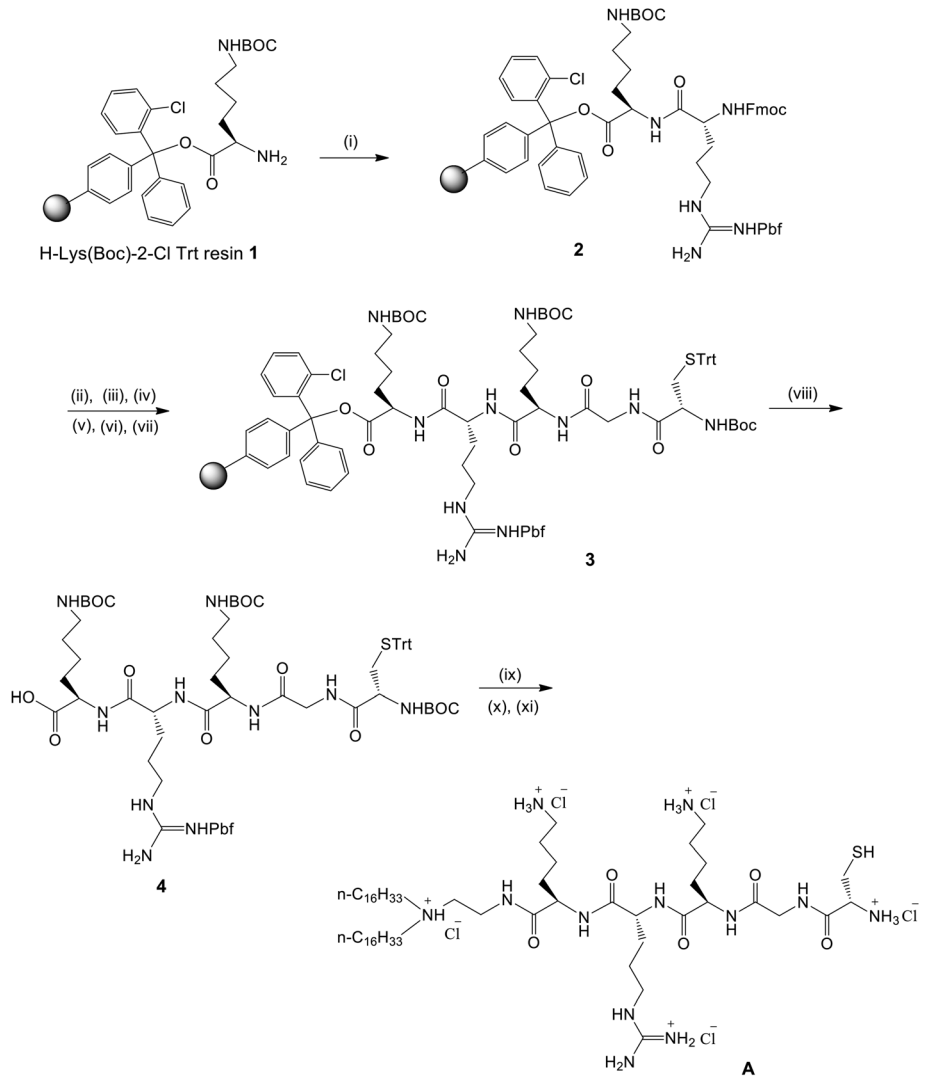

Fig. 2 Solid phase synthesis of the CGKRK-lipopeptide (CLP). Reagents: (i) Fmoc-Arg(Pbf)-OH (2 equiv.), HATU (2 equiv.), DIPEA (4 equiv.), rt, 1 × 30 min, and then 1 × 1 h (ii) piperidine-DMF (1 : 4), rt, 4 min, (×2); (iii) Fmoc-Lys(BOC)-OH (2 equiv.), HATU (2 equiv.), DIPEA (4 equiv.), rt, 1 × 30 min, and then 1 × 1 h (iv) piperidine-DMF (1 : 4), rt, 4 min, (×2); (v) Fmoc-Gly-OH (2 equiv.), HATU (2 equiv.), DIPEA (4 equiv.), rt, 1 × 30 min, and then 1 × 1 h; (vi) piperidine-DMF (1 : 4), rt, 4 min, (×2); (vii) BOC-Cys(Trt)-OH (2 equiv.), HATU (2 equiv.), DIPEA (4 equiv.), rt, 1 × 30 min, and then 1 × 1 h; (viii) TFA-Dry DCM (0.5%), 2 h, 0 °C; (ix) *N*,*N*-di-*n*-hexadecyl-N-2-aminoethylamine, dry DCM, EDCI, HOBt, 12 h; (x) TFA–thioanisole–ethanedithiol–anisole (90 : 5 : 3 : 2), 3 h, 0 °C; and (xi) Cl^{-} ion exchange (Amberlyst resin).

for 30 min) containing EDCI (8.2 mg, 0.042 mmol), HOBT (6.4 mg, 0.042 mmol) and the protected penta-peptide intermediate **4** (0.058 g, 0.042 mmol) in dry DCM (5 mL). The resulting solution was left under stirring at room temperature for 12 h. Then the solvent was evaporated using a rotary evaporator at 30 °C and the residue was dried completely under high vacuum. The dried intermediate was treated with TFA–thioanisole–ethanedithiol–anisole (90 : 5 : 3 : 2 v/v, 2 mL) for 3 h at 0 °C and washed with TFA : DCM (1 : 9, v/v, 8 mL). The acid washings were concentrated to about 1 mL and Et_2O was added until a white precipitate separated. The precipitate upon chloride ion exchange chromatography over Amberlyst IRA-400 resin afforded the target CGKRK-lipopeptide (CPL, Fig. 1) as a white, fluffy solid (25 mg, 55% based on intermediate **4**). The purified CGKRK-lipopeptide was found to be essentially insoluble in chloroform and could be dissolved in 3 : 1 (v/v) methanol : chloroform. The ^{1}H NMR spectra of the pure CGKRK-lipopeptide was thus recorded in $CD_3OD/CDCl_3$ (3/1, v/v) mixed solvent (Fig. S1A, ESI‡). The final CGKRK-lipopeptide was characterized by the molecular ion peak (C in ESI-MS) (Fig. S1B, ESI‡) and the purity was confirmed by reversed phase analytical HPLC using two different mobile phases (Fig. S2, ESI‡).

^{1}H NMR (200 MHz, $CDCl_3$ + CD_3OD): δ/ppm = 0.9 [t, 6H, $C\underline{H}_3$–$(CH_2)_{15}$–]; 1.1–1.5 [bs, 56H, –$(C\underline{H}_2)_{14}$–; m, 6H, Lys $C^{\beta}\underline{H}_2$ + Arg $C^{\beta}\underline{H}_2$]; 1.5–2 [m, 8H, Lys $C^{\gamma}\underline{H}_2$ + Lys $C^{\delta}\underline{H}_2$; m, 2H, Arg $C^{\gamma}\underline{H}_2$; m]; 2.5–3.2 [m, 4H, –N(–$C\underline{H}_2$–CH_2–)$_2$; m, 2H, –N–$C\underline{H}_2$–CH_2– NH–CO; m, 4H, Lys $C^{\omega}\underline{H}_2$; m, 2H, Arg $C^{\delta}\underline{H}_2$; m, 2H, Cys $C^{\beta}\underline{H}_2$]; 3.3–3.8 [m, 2H, –N–CH_2–$C\underline{H}_2$–NH–CO–; m, 2H, Lys$C^{\alpha}\underline{H}$; m, 1H, Cys $C^{\alpha}\underline{H}$; m, 1H, Arg $C^{\alpha}\underline{H}$]; 4.4–4.5 [m, 2H, Gly $C^{\alpha}\underline{H}_2$]. ESI-MS: m/z = 1082 $[M]^+$.

Preparation of liposomal formulations. Cationic liposomes of CGKRK-lipopeptide **1** (CLP, Fig. 1) were prepared using cholesterol and $(n\text{-}C_{16}H_{33})_2N^+(CH_3)CH_2CH_2N^+(CH_3)_3$ $2Cl^-$ (a readily available di-cationic amphiphile in our laboratory commonly used for enhancing the transfection efficiencies of receptor selective cationic lipopeptides) as co-lipids maintaining lipopeptide : dicationic amphiphile : cholesterol mole ratios of 0.25 : 1 : 0.5. To prepare liposomal formulations containing WP1066, the stock solution of WP1066 was prepared by dissolving it in chloroform (5 mg mL^{-1}). The final total lipid : WP1066 ratio (w/w) used in preparing the liposomal formulations containing only WP1066 and formulations containing both WP1066 and STAT3 siRNA was 10 : 1 for both *in vitro* and *in vivo* experiments. The appropriate lipid mixtures were dissolved in a mixture of chloroform and methanol (3 : 1, v/v) in a glass vial and the solvent was removed with a thin flow of moisture-free nitrogen gas. The dried lipid film was then kept under high vacuum for 8 h and hydrated overnight either in autoclaved water to prepare liposomal formulations containing only WP1066 or in nuclease free water containing a siRNA–protamine complex (total lipid : siRNA w/w 25 : 1, siRNA : protamine w/w 1 : 10) to prepare liposomal formulations containing either only siRNA or both siRNA and WP1066. The hydrated lipid film was first vortexed for 1–2 minutes at room temperature to produce multi-lamellar vesicles (MLVs). For liposomes having only WP1066, MLVs were then sonicated in an ice bath until clarity using a Branson 450 sonifier at 100% duty cycle and 25 W output power to produce small unilamellar vesicles (SUVs). For liposomes having siRNA, MLVs were bath-sonicated for 1 min to produce small unilamellar vesicles (SUVs) and then frozen and thawed 16–20 times at −78 °C to achieve equilibrium transmembrane solute distributions. Unentrapped siRNA was eluted by using Amicon Ultra centrifugal filter units (10 kD), and the liposomes were finally concentrated using Amicon Ultra centrifugation to prepare a final lipid concentration of 1 mM for the *in vitro* experiments or 5 mM for the *in vivo* experiments. In the case of FITC labeled siRNA, the concentration of siRNA entrapped in liposomes was measured by lysing the liposomes with 1% Triton-X and using fluorescence measurement from a standard graph of FITC labeled siRNA.

Liposomes of the *in vivo* DC-targeting cationic lipid (CL, Fig. 1) were prepared using DOPE as a co-lipid maintaining DOPE : CL mole ratios of 1 : 1. The appropriate lipid mixtures were dissolved in a mixture of chloroform and methanol (3 : 1, v/v) in a glass vial and the solvent was removed with a thin flow of moisture free nitrogen gas. The dried lipid film was then kept under high vacuum for 8 h and hydrated overnight in autoclaved water. The hydrated lipid film was first vortexed for 1–2 min at room temperature to produce multi-lamellar vesicles (MLVs). MLVs were then sonicated in an ice bath until clarity using a Branson 450 sonifier at 100% duty cycle and 25 W output power to produce small unilamellar vesicles (SUVs).

Preparation of plasmid DNA. pCMV-MART1 plasmid DNA was obtained as a kind gift from Dr Van den Eynde, Ludwig Institute for Cancer Research, Brussels, Belgium and pCMV-SPORT-β-gal and p-CMV-GFP plasmids were generous gifts from Dr Nalam Madhusudhana Rao of Centre for Cellular and Molecular Biology, Hyderabad, India. Plasmids were amplified in the DH5a strain of *Escherichia coli*, isolated by an alkaline lysis procedure and finally purified by PEG-8000 precipitation as described previously.[26] The purity of the plasmid was checked by A260/A280 ratio (around 1.9) and 1% agarose gel electrophoresis.

Zeta potential (ξ) and size measurements. The sizes and the global surface charges (zeta potentials) of liposomal WP1066, liposomally encapsulated STAT3 siRNA and liposomes containing both WP1066 and STAT3 siRNA were measured by photon correlation spectroscopy and electrophoretic mobility on a Zeta sizer 3000HS_A (Malvern, UK). The sizes were measured in deionised water (nuclease free water for liposomes containing siRNA) with a sample refractive index of 1.59 and a viscosity of 0.89. The system was calibrated by using a 200 nm ± 5 nm polystyrene polymer (Duke Scientific Corp., Palo Alto, CA). The diameters of liposomes and liposomal curcumin were calculated by using the automatic mode. The zeta potential was measured using the following parameters: viscosity, 0.89 cP; dielectric constant, 79; temperature, 25 °C; F(Ka), 1.50 (Smoluchowski); maximum voltage of the current, 15 V. The system was calibrated by using a DTS0050 standard from Malvern, UK. Measurements were done 10 times with the zero

field correction. The surface potentials were calculated by using the Smoluchowski approximation.

Cellular uptake studies. In B16F10 cells, cellular uptake of liposomes containing CGKRK-lipopeptide **1** was examined by labeling the liposome with Rho-PE (0.1 mol% with respect to the dicationic amphiphile). Cells were seeded at a density of ~10 000 cells per well in a 96-well plate for 18–24 h and Rho-PE labeled liposomes containing the CGKRK-lipopeptide (CLP, Fig. 1) were added to each well. The total volume in each well was made up to 100 μL with complete medium. After 3 h of treatment, cells were washed with phosphate buffered saline and the live B16F10 cells were viewed using an epifluorescence microscope. To analyze the cellular uptake of FITC-labeled siRNA encapsulated in the liposomes of the CGKRK-lipopeptide (CLP, Fig. 1), HUVEC and B16F10 cells were seeded at a density of ~10 000 cells per well in a 96-well plate for 18–24 h before the treatment and liposomally encapsulated FITC-siRNA (30 nM) was added to each well. The total volume in each well was made up to 100 μL with serum-free medium. After 3 h of treatment, cells were washed with phosphate buffered saline and the live cells were viewed using an epifluorescence microscope.

Apoptosis analysis by flow cytometry. HUVEC and B16F10 cells were seeded at a density of ~3×10^5 cells per well in a 6-well plate for 18–24 h before the treatment. Cells were treated (4 h) with: WP1066 (2 μM) entrapped in the liposomes of CLP, STAT3 siRNA (20 nM) encapsulated in the liposomes of CLP, both WP1066 (2 μM) and STAT3 siRNA (20 nM) encapsulated in the liposomes of CLP and scrambled siRNA (20 nM) encapsulated in the liposomes of CLP in a total 1.5 mL of DMEM for B16F10 and EBM2 (serum free) media in the case of HUVEC cells. After 4 h of incubation at 37 °C, the media were completely replaced by 2 mL of DMEM containing 10% FBS for B16F10 cells and 2 mL of complete EBM2 for HUVEC cells. After 24 h of treatment, cells were trypsinized, washed with PBS and centrifuged and the pellets were resuspended in 500 μL of binding buffer containing annexin-V FITC (0.25 μg) and PI (1.0 μg). The mixture was incubated for 15 min in the dark and analyzed using a flow cytometer (BD FACS Canto II).

RT-PCR (reverse transcription-PCR) analysis. A semi-quantitative RT-PCR analysis was performed to measure the levels of various gene expressions in both treated cells and untreated cells. HUVEC and B16F10 cells were seeded at a density of ~1×10^6 cells in a T25 flask for 18–24 h before the treatment. Cells were treated with the targeted liposome containing 2 μM WP1066, targeted liposome containing 20 nM STAT3 siRNA, targeted liposome containing 2 μM WP1066 and 20 nM STAT3 siRNA and targeted liposome containing 20 nM scrambled siRNA in 3 mL of DMEM for B16F10 and EBM2 (serum free) media in the case of HUVEC cells for 4 h. After incubation of the cells under a humidified atmosphere containing 5% CO_2 at 37 °C for 4 h, the media were completely removed by 3 mL of DMEM containing 10% FBS for B16F10 cells and 3 mL of complete EBM2 medium for HUVEC cells. After 24 h of the treatment, total RNA were extracted from the treated and untreated cells using the TRIzol reagent. First-strand cDNAs were synthesized from the corresponding mRNAs by a reverse transcription reaction according to the manufacturer's instructions (Reverse Transcription System, Promega, USA). cDNAs were amplified using the PCR Master Mix (Promega, USA) and the forward and reverse primers (BioTek Desk, USA). The amplified sequences were finally resolved in 2% agarose gel electrophoresis and visualized using 0.1% ethidium bromide under UV light.

Western blot analysis. HUVEC and B16F10 cells were seeded at a density of ~1×10^6 cells in a T25 flask for 18–24 h before the treatment. Cells were treated with the targeted liposome containing 2 μM WP1066, targeted liposome containing 20 nM STAT3 siRNA, targeted liposome containing 2 μM WP1066 and 20 nM STAT3 siRNA and targeted liposome containing 20 nM scrambled siRNA in 3 mL of DMEM for B16F10 and EBM2 (serum free) media in the case of HUVEC cells for 4 h. After incubation of the cells under a humidified atmosphere containing 5% CO_2 at 37 °C for 4 h, the media were completely removed by 3 mL of DMEM containing 10% FBS for B16F10 cells and 3 mL of complete EBM2 medium for HUVEC cells. After 24 h of the treatment, the cells were detached from the flask using a cell scrapper and the cells were lysed with a lysis reagent (CCLR, Promega) at 4 °C. The total protein contents of the cell lysates were quantified by the BCA assay method and 80 μg of total proteins were dissolved in an SDS-PAGE sample buffer prior to separation by 12% SDS-PAGE. Proteins were transferred to a nitrocellulose membrane (Hybond-ECL, Amersham Biosciences, NJ) using wet blotting. Membranes were blocked for 2 h at room temperature with 5% non-fat milk in PBS containing 0.05% Tween-20 (PBS-T). Blots were then incubated with Rabbit Polyclonal PhosphoDetect anti-STAT3, rabbit polyclonal anti-STAT3 and rabbit polyclonal anti β-actin (as loading controls) primary antibodies at 1 : 1000 dilutions (in 10 mL 0.05% PBS-T) overnight at 4 °C. After washing with PBS-T (3 × 10 mL, 10 min each), the membranes were incubated with a goat anti-rabbit secondary antibody conjugated to alkaline phosphatase (in 10 mL 0.05% TBS-T with 1 : 5000 dilution) for 2 h. Protein bands were developed using a BCIP/NBT chromogen solution (Calbiochem) and the expression levels were normalized to β-actin.

Microscopic imaging of FITC labeled siRNA uptake in tumor vasculature. ~1.5×10^5 B16F10 cells in 250 μL of Hank's buffer salt solution (HBSS) were injected in the right flank of four 6–8 weeks old C57BL/6J mice (n = 2). After 18 d, when the tumor volume reached ~1500 mm^3, mice were injected intravenously with a single dose of FITC labeled siRNA (3 μg per mouse) encapsulated in the liposomes of the CGKRK-lipopeptide (CLP, Fig. 1) in a total ~250 μL of 5% glucose. After 24 h, mice were sacrificed and tumors were excised. 10 micron thick tumor cryosections were taken on a glass slide using a cryostat instrument (Leica). The slides were fixed in 4% formaldehyde in PBS. The fixed slides were then stained with a blood vessel marker, vWF (von Willebrand factor) available in a blood vessel staining kit (Chemicon, USA) according to the manufacturer's protocol. The stained slides were placed under an inverted fluorescence microscope and images were taken in a

bright field for the blood vessel and images were taken in a green field for the FITC labeled siRNA.

Biodistribution of FITC labeled siRNA. ~1.5×10^5 B16F10 cells in 250 μL of HBSS were injected in the right flank of 6–8 weeks old C57BL/6J mice (n = 2). After 18 d, when the tumor volume reached ~1500 mm^3, mice were injected intravenously with a single dose of FITC labeled siRNA (6 μg per mouse) encapsulated in the liposomes of the CGKRK-lipopeptide (CLP, Fig. 1) in a total ~250 μL of 5% glucose. 24 h post injection, the tumors and tissue samples were obtained. The samples were suspended in cold PBS. 300 μL of lysis buffer (0.1 M Tris-HCl, 2 mM EDTA and 0.2% Triton X-100, pH 7.8) was added to each organ and homogenized using a mechanical homogenizer. The homogenates were centrifuged at 14 000 rpm for 20 minutes at 4 °C and 100 μL of the supernatants were taken in each well of a 96-well plate in doublet. Concentrations of FITC labeled siRNA present in the samples were measured by fluorescence measurements from a standard graph of fluorescence *vs.* the FITC labeled siRNA concentration. Background fluorescence from the tissue extracts, if any, were corrected by subtracting the fluorescence of the tissue extracts from the untreated control mice.

Tumor growth inhibition study. ~1.5×10^5 B16F10 melanoma cells in 250 μL of HBSS were s.c. injected in the right flank of 6–8 weeks old female C57BL/6J mice (each weighing 20–22 g) on day 0. On day 14, tumor bearing mice were randomly sorted into six groups and each group (n = 5) was administered intravenously with the targeted liposome containing both STAT3 siRNA (2 μg per mouse) and WP1066 (10 mg per kg BW of mice), targeted liposome containing WP1066 (10 mg per kg BW of mice), targeted liposome containing STAT3 siRNA (2 μg per mouse), targeted liposome containing scrambled siRNA (2 μg per mouse) and targeted liposome containing both WP1066 (10 mg per kg BW of mice) and scrambled siRNA (2 μg per mouse) on days 14, 16, 19, 21 and 23. The sixth group (n = 5) was intravenously injected with vehicle (5% aqueous glucose). Tumor volumes ($V = \frac{1}{2}ab^2$, where a = maximum length of the tumor and b = minimum length of the tumor measured perpendicular to each other) were measured using a slide calipers for up to 23 d.

Targeted chemotherapy and immunotherapy. ~1.5×10^5 B16F10 melanoma cells in 250 μL of HBSS were s.c. injected in the right flank of 6–8 weeks old female C57BL/6J mice (each weighing 20–22 g) on day 0. On day 14, mice were randomly sorted into six groups. The first and second groups (n = 5) were administered intravenously with vehicle (5% aqueous glucose) and the liposomes of CGKRK-lipopeptide **1** (without siRNA or WP1066), respectively. The 3rd, 4th and 5th groups (n = 5) were administered intravenously with STAT3 siRNA (2 μg per mouse) and WP1066 (10 mg per kg BW of mice) co-encapsulated in the liposomes of CGKRK-lipopeptide **1** on days 14, 16, 18, 21 and 23. The 4th group was also injected (s.c.) with the lipoplexes of pCMV-β-gal and liposomes of lysinylated cationic amphiphiles with guanidine and mannose-mimicking shikimoyl head-groups (cationic amphiphile **2**) on days 15, 17 and 19 (using 200 μL of 5% glucose solution containing 15 μg of DNA, 4 : 1 lipid : DNA charge ratio for each mouse). Both 5th and 6th groups were immunized (s.c.) with the lipoplexes of p-CMV-MART1 and the liposomes of lysinylated cationic amphiphiles with guanidine and mannose-mimicking shikimoyl head-groups (cationic amphiphile **2**) on days 15, 17 and 19 (using 200 μL of 5% glucose solution containing 15 μg of DNA, 4 : 1 lipid : DNA charge ratio for each mouse). Tumor volumes ($V = \frac{1}{2}ab^2$, where a = maximum length of the tumor and b = minimum length of the tumor measured perpendicular to each other) were measured using a slide calipers.

Statistical analysis. Error bars represent mean values ± SEM. The statistical significance of the experiments was determined by a two-tailed Student's test. $^*P < 0.05$ was considered statistically significant.

Immunohistochemical studies. After five injections on days 14, 16, 19, 21 and 23, tumors were excised 24 h post the last injection, frozen in a cryostat at −30 °C for 2 h and cryosectioned, and ten micrometer frozen cryosections were fixed in a 4% methanol free formaldehyde solution for 30 min. The fixed tumor sections were washed twice with PBS for 5 min and were immunostained for observing VE-cadherin positive endothelial cells and and TUNEL positive apoptotic cells. The stained tumor cryosections were observed in the same positions using a fluorescence microscope (×10 magnification) using green (for TUNEL) and red (for VE-cadherin) filters and in a bright field when immunostained for vWF, a marker of tumor endothelial cells. Frozen tumor sections were also immunostained with a CD31 primary antibody (at 1 : 100 dilution) in PBS for 30 min and then with a goat anti-rabbit HRP-conjugated secondary antibody (at 1 : 100 dilution) for 15 min to mark the tumor endothelial microvessels. Tumor slides stained with CD31 were observed in a bright field using an inverted microscope (×20 magnification).

Inhibition of STAT3 phosphorylation *in vivo*. ~1.5×10^5 B16F10 melanoma cells in 100 μL of HBSS were s.c. injected in the right flank of 6–8 weeks old female C57BL/6J mice (each weighing 20–22 g) on day 0. On day 14, mice injected with B16F10 cells were randomly sorted into six groups and each group (n = 5) was administered intravenously with the targeted liposome containing both STAT3 siRNA (2 μg per mouse) and WP1066 (10 mg per kg BW of mice), targeted liposome containing WP1066 (10 mg per kg BW of mice), targeted liposome containing STAT3 siRNA (2 μg per mouse), targeted liposome containing scrambled siRNA (2 μg per mouse) and targeted liposome containing both WP1066 (10 mg per kg BW of mice) and scrambled siRNA (2 μg per mouse) on days 14, 16, 19, 21 and 23. The sixth group (n = 5) was intravenously injected with vehicle (5% aqueous glucose). On day 24, mice were sacrificed, tumors were excised and B16F10 cells were isolated from the tumors of each group. The cell lysates were prepared by lysing the cells with a lysis reagent (CCLR, Promega, USA) at 4 °C and subjected to the western blot experiment as discussed above.

***In situ* IFN-γ and IL-4 ELISA assays.** IFN-γ and IL-4 ELISA assays were done as described previously.[29] One week after the last immunization process, mice were sacrificed and their spleens were collected. Splenocytes were isolated by mincing

the spleens with a syringe plunger and the erythrocytes were lysed with 1 mL of a lysis buffer (0.14 M ammonium chloride in 0.02 M Tris-HCl, pH 7.2). The viable cells were counted and used for the IFN-γ and IL-4 ELISA assays (without any *in vitro* re-stimulation and after three days of stimulation). The assay was performed according to the manufacturer's protocol (endogen mouse IFN-g ELISA kit and mouse IL-4 ELISA kit, Pierce Biotechnology, USA). Briefly, splenocytes were incubated in 96-well plates pre-coated with anti-mouse IFN-γ or anti-mouse IL-4 antibodies at 1×10^6 cells per well in 50 mL of complete medium. The plates were covered and incubated for 12 h at 37 °C in the presence of 5% CO_2. The cells were then washed out with a wash buffer (3 × 200 mL), and 50 mL of a biotinylated secondary antibody was added to each well and incubated for 1 h at room temperature. The plates were washed with a wash buffer (3 × 200 mL) and incubated with 100 mL of streptavidin–HRP solution for 30 min. The plates were again washed with a wash buffer (3 × 200 mL), treated with 100 mL of TMB substrate solution and incubated for 30 min in the dark. The reaction was stopped by adding 100 mL of a stop solution and the absorbance was measured using a microplate reader at 450 nm.

CTL assay. CTL assays were performed following a previously described method.[29] Briefly, single-cell suspensions of spleen cells were prepared from mice one week after the second booster dose, seeded onto 6-well (~1×10^7 cells per well) plates and cultured with B16F10 cells (~1×10^6 cells per well) in RPMI complete medium containing 100 U mL^{-1} antibiotic solution (Sigma, USA) and 50 U ml^{-1} IL-2 (Thermo Fisher Scientific, USA). These were then used as effector cells. Ten-thousand fresh target B16F10 cells were incubated with increasing numbers of effector cells (10 : 1 to 100 : 1) in each well of U-bottomed 96-well plates for 6 h at 37 °C under 5% CO_2, and then the lactate dehydrogenase (LDH) levels in the cell culture supernatants were measured according to the manufacturer's protocol (Promega, USA).

Results and discussion

Chemistry

CGKRK-lipopeptide **1** (CLP, Fig. 1) was synthesized by using a conventional Fmoc strategy-based solid phase peptide synthetic route as shown schematically in Fig. 2. The details of the synthetic schemes, procedures, nuclear magnetic resonance (NMR), and mass spectral data for CLP as well as the high performance liquid chromatography (HPLC) profiles of the purified lipopeptide in the two different mobile phases are provided in the ESI (Fig. S1A, S1B and S2,‡ respectively). The *in vivo* DC-targeting lipid containing both guanidine and mannose-mimicking shikimoyl head-groups (CL, Fig. 1) was synthesized as described previously.[29]

Hydrodynamic sizes and zeta potentials (ξ) of liposomes

Hydrodynamic diameters and the global surface charges (zeta potentials) of the liposomal formulations containing only STAT3 siRNA, only WP1066 and both STAT3 siRNA and WP1066 were measured by photon correlation spectroscopy and electrophoretic mobility using a Zeta sizer $3000HS_A$ (Malvern, UK). The liposomal sizes and surface potentials for all these three formulations were found to be within the range of 180–210 nm and 4–6 mV, respectively (Table S1, ESI‡).

Apoptosis of endothelial and tumor cells

Toward probing the synergistic effects of the presently described liposomal formulations of STAT3 siRNA and WP1066 in inducing apoptosis in endothelial cells, we studied the conventional Annexin V/propidium iodide (PI) binding-based flow cytometric apoptosis assay. Incubation of HUVEC cells with liposomal formulations of CLP containing both STAT3 siRNA and WP1066 induced significantly enhanced accumulation of late apoptotic cells compared to the late apoptotic populations in HUVEC cells treated with liposomal formulations containing only WP1066 and only STAT3 siRNA (Fig. 3A). Importantly, scrambled siRNA encapsulated in the liposomes of CGKRK-lipopeptide **1** was found to be incompetent to induce apoptosis in endothelial cells (Fig. 3A). Consistently, similar synergistic effects of liposomally co-loaded STAT3 siRNA and WP1066 in inducing enhanced apoptosis were also observed in the tumor (B16F10) cells (Fig. S3, ESI‡).

RT-PCR and western blot analysis

With a view to analyze the effects of combined therapeutics co-loaded in CLP liposomes on the mRNA expressions of genes involved in the STAT3 signaling pathway, RT-PCR experiments were performed. The decrease in the expressions of anti-apoptotic genes such as VEGF, STAT3, Bcl2, and $BclX_L$ genes as well as the increase in expression of the pro-apoptotic caspase-3 gene were observed when compared with the loading control β-actin in both HUVEC (Fig. 3B, the original gel images used for drawing Fig. 3B are provided in Fig. S4‡) and B16F10 (Fig. S5A, ESI, the original gel images used for drawing Fig. S5A are provided in Fig. S6‡) cells. Collectively, the findings in the RT-PCR experiments (Fig. 3B and Fig. S5A, ESI‡) showed that liposomally entrapped combined therapeutics (STAT3 siRNA + WP1066) were more potent in downregulating the transcription of anti-apoptotic genes and upregulating the transcription of pro-apoptotic genes compared to their levels in cells treated with liposomally entrapped individual therapeutics (either STAT3 siRNA or WP1066). Importantly, liposomally encapsulated scrambled siRNA showed no effect on genes involved in the STAT3 signaling pathway (Fig. 3B and Fig. S5A, ESI‡). To examine the possible inhibition of STAT3 phosphorylation, HUVEC and B16F10 cells were treated with liposomal formulations containing chemotherapeutics, and cell lysates (proteins) were subjected to western blot analysis. Liposomal formulations of combined therapeutics (STAT3 siRNA and WP1066) were found to be more efficient in down-regulating the expressions of STAT3 and p-STAT3 protein levels compared to their levels in the cells treated with liposomally entrapped individual therapeutics (either STAT3 siRNA or

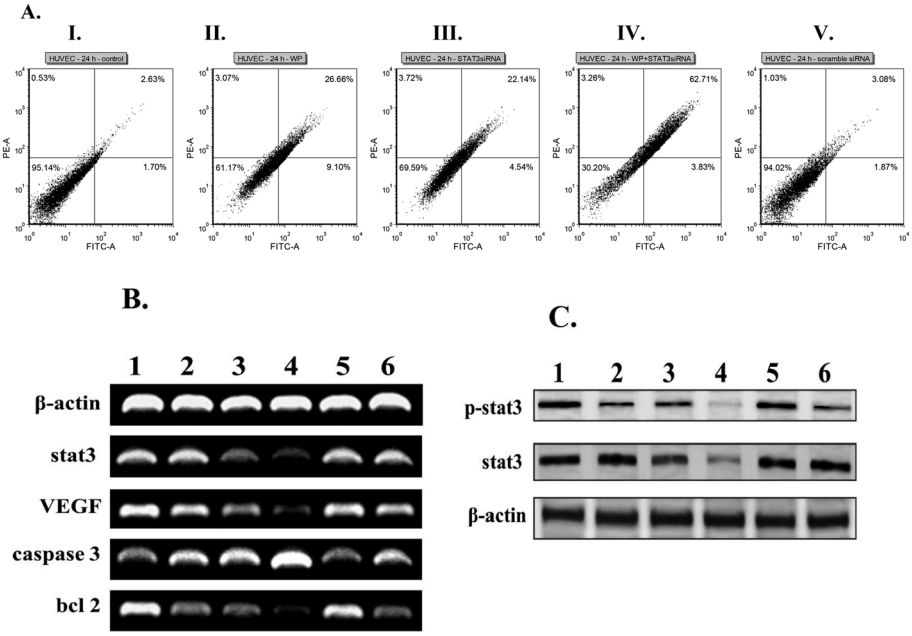

Fig. 3 Synergistic effects of STAT3 siRNA and WP1066 co-loaded liposomes of CLP in inducing apoptosis and inhibiting STAT3 activation in endothelial cells. (A) Untreated control HUVEC (I); HUVEC treated with only WP1066-loaded liposomes of CLP (II); HUVEC treated with only STAT3 siRNA-loaded liposomes of CLP (III); HUVEC treated with STAT3 siRNA and WP1066 co-loaded liposomes of CLP (IV); and HUVEC treated with scrambled siRNA loaded liposomes of CLP (V). Both untreated (I) and treated cells were stained with FITC-Annexin V and propidium iodide (PI) for the flow cytometric analysis. The horizontal and vertical axes represent cells labeled with FITC-Annexin V and PI, respectively in the dot plot. Dots in the upper right quadrant represent late apoptotic cells (positive for both Annexin V and PI). (B and C) mRNA levels (B) of the indicated genes involved in the STAT3 signalling pathway; the levels of STAT3 and p-STAT3 protein expressions (C) were measured by RT-PCR and western blotting, respectively. Lane 1, untreated cells; lane 2, cells treated with the targeted liposomal WP1066; lane 3, cells treated with the targeted liposome containing STAT3 siRNA; lane 4, cells treated with the targeted liposome containing both WP1066 and STAT3 siRNA; lane 5, cells treated with the targeted liposome containing scrambled siRNA; and lane 6, cells treated with the targeted liposome containing both WP1066 and scrambled siRNA.

WP1066) in both endothelial and tumor cells (Fig. 3C and Fig. S5B, ESI‡). An important observation needs further clarification at this point of discussion. As mentioned above, activated (phosphorylated) JAKs catalyze phosphorylation of the STAT proteins bound to the phosphorylated intracellular domains of the cytokine receptors.[46,49] Thus, WP1066, the inhibitor of JAK2, decreases the level of pSTAT3 protein in cells treated with liposomal formulations containing only WP1066 (compared to the level of pSTAT3 protein in the untreated control cells). Since lesser pSTAT3 would be produced in JAK2-catalyzed phosphorylation of STAT3 proteins in the cells treated with liposomal formulations containing only WP1066, in a quantitative study, one may observe a somewhat increased level of STAT3 proteins (not a decreased level) after such treatment of cells. However, in qualitative PCR and western blot experiments (Fig. 3B and C), depending on the degree of JAK2 inhibition by WP1066, we may not always be able to see the enhanced levels of STAT3 proteins in cells treated with liposomal formulations containing only WP1066. Such a possibility could play a role in the decreased pSTAT3 level (compared to the pSTAT3 level in the untreated cells, lane 2, Fig. 3C) and no significant changes in the STAT3 protein levels (lane 2, Fig. 3B and C) observed in the cells treated with liposomal formulations containing only WP1066.

Targeting FITC labeled siRNA to tumor vasculature

With a view to evaluate the efficiency of liposomes of CLP to deliver encapsulated siRNA in tumor vasculature, we intravenously administered FITC-labeled siRNA encapsulated in the liposomes of CLP in C57BL/6J mice bearing aggressive B16F10 tumors. Immunohistochemical staining of fixed tumor cryosections (prepared 24 h post the liposome injection) using antibodies against vWF (tumor vasculature marker) revealed co-localization of FITC (green) and tumor endothelial cells (Fig. S7, ESI‡). Thus, the findings summarized in Fig. S7‡ indicate that the liposomes of CLP deliver its entrapped siRNA cargo to tumor endothelial cells.

Biodistribution of liposomally encapsulated FITC-labeled siRNA

Toward examining the tissue distribution profiles of the presently described liposomal systems, FITC-labeled siRNA encapsulated in the liposomes of CLP was intravenously administered in mice bearing B16F10 melanoma tumors. After 24 h of treatment, tumors and tissue samples were obtained to quantify the concentration of FITC-labeled siRNA in each sample. Importantly, the concentration of FITC labeled siRNA in the tumor was found to be remarkably higher than those in the other body tissues including the lungs, liver, kidneys, spleen

and heart (Fig. S8, ESI‡). Autofluorescence intensities for each organ of the untreated control mice were subtracted from the corresponding measured values in the organs of the treated mice for constructing the biodistribution profile (Fig. S8‡). The fluorescence and autofluorescence intensities measured for each organ used for drawing Fig. S8‡ are provided in an Excel Sheet format in Table S2, ESI.‡

Tumor growth inhibition study using tumor-selective CLP liposomes

With a view to evaluate the therapeutic potential of the synergistic use of WP1066 and STAT3 siRNA encapsulated in the presently described liposomes of CLP, C57BL/6J mice bearing aggressive B16F10 tumors were separately administered (i.v.) with liposomal formulations of CLP containing only WP1066, only STAT3 siRNA and both WP1066 and STAT3 siRNA. Pronounced tumor growth inhibition was observed in mice treated with formulations containing both the therapeutics (Fig. 4A and B, the original colored images of the tumors shown in Fig. 4B are provided in Fig. S9, ESI‡). Comparatively, tumor growth inhibition was found to be 2–3 fold less in mice treated with formulations containing only WP1066 or only STAT3 siRNA (Fig. 4A and B). Mice intravenously administered with vehicle alone (in 5% aqueous glucose solution) developed large tumors on day 23 (Fig. 4A and B) and were sacrificed on day 24 post tumor inoculation.

Apoptosis in tumor vasculature

Since liposomes of CLP were found to be efficient in targeting siRNA to tumor vasculatures (Fig. S8, ESI‡), we envisaged that the observed tumor growth inhibition (Fig. 3A and B) presumably resulted from the apoptosis of tumor endothelial cells. To confirm this, C57BL/6J mice bearing aggressive murine B16F10 melanoma tumors were administered liposomal formulations having both WP1066 and STAT3 siRNA. On day 24, mice were sacrificed, and tumors were cryosectioned, fixed and immunostained for VE-cadherin (another endothelial cell marker). The same tumor cryosections were also stained using TUNEL assay kits for labeling apoptotic cells. The colocalization of the TUNEL-positive and VE-cadherin-positive cells in the tumor cryosections (Fig. 4C, the original snapshots are provided in Fig. S10 and S11, ESI‡) was consistent with the proposition that the remarkable tumor growth inhibition properties of liposomal formulations of CLP containing co-loaded WP1066 and STAT3 siRNA are presumably mediated through apoptosis of tumor endothelial cells. Toward confirming the efficiencies of the presently described liposomal formulations of the CGKRK-lipopeptide containing WP1066 and STAT3 siRNA in inhibiting the formation of microvessels around tumor tissues, tumor cryosections were immunostained with CD31 (one of the most widely used markers of tumor endothelial cells) antibodies. The findings in these immunohistochemical staining experiments clearly showed least tumor microvessel densities in the tumor cryosections from mice treated with liposomal formulations containing both WP1066 and STAT3 siRNA (Fig. S12‡).

Inhibition of STAT3 phosphorylation *in vivo*

To examine the possible inhibition of STAT3 phosphorylation under *in vivo* conditions, B16F10 tumor cells were isolated from mice treated with chemotherapeutics encapsulated in liposomes of CLP. Most significant decrease in STAT3 activation at the protein level was observed in B16F10 cells isolated from tumors treated with STAT3 siRNA and WP1066 co-encapsulated in the liposomes of CGKRK-lipopeptide **1** (Fig. S13, ESI‡). Importantly, liposomally encapsulated scrambled siRNA showed no effect on the STAT3 and p-STAT3 protein levels *in vivo* (Fig. S13, ESI‡).

Combined effects of tumor-selective chemotherapy and *in vivo* DC-targeted genetic immunization on tumor growth inhibition

Toward evaluating the therapeutic promise of the present combination approach in inhibiting the established mouse melanoma, mice were immunized (s.c.) after two weeks of tumor inoculation with lipoplexes of a melanoma antigen encoded DNA vaccine (p-CMV-MART1) and direct *in vivo* DC-targeting liposomes of CL (Fig. 1) on days 15, 17 and 19 post tumor inoculation. Tumor growth inhibition studies (Fig. 4A) suggest that only genetic immunization (without using any tumor-selective chemotherapy) is not enough to inhibit tumor growth. Most notably, complete regression of the established melanoma tumor was observed only when established melanoma-bearing mice were treated with five WP1066 and STAT3 siRNA co-loaded tumor-selective CLP liposomes in combination with three s.c. genetic immunization with melanoma antigen (MART1) encoded p-CMV-MART1 DNA vaccines complexed with *in vivo* DC-targeting liposomes of CL (Fig. 4E and F) following the treatment schedules shown in Fig. 4D.

Melanoma-specific cellular immune response

Toward examining the role of cellular immune responses in the presently described combination approach, we conducted a cytotoxicity (CTL) assay and measured the amounts of secreted IFN-γ and IL-4 when effector cells (splenocytes isolated from immunized mice) were incubated with target B16F10 melanoma cells. Primed splenocytes were collected and used for lysing the target melanoma cells across the effector : target cell ratios of 10 : 1–100 : 1. The effector splenocytes isolated from mice receiving the combined treatment were significantly more efficient in lysing the target melanoma cells than those isolated from mice treated (s.c.) with only lipoplexes of p-CMV-MART1 and CL or with only STAT3 siRNA and WP1066 co-loaded liposomes of CLP (Fig. S14A, ESI‡). Thus, the findings summarized in Fig. S14A‡ demonstrate that the use of genetic immunization in combination with targeted chemotherapy is most efficient to induce formations of anti-B16F10 specific CTLs. Using an ELISA-based protocol, we measured the relative amounts of IFN-γ and IL-4 in the supernatant of the overnight co-culture of the target cells B16F10 and splenocytes of the treated mice. Consistently, results in

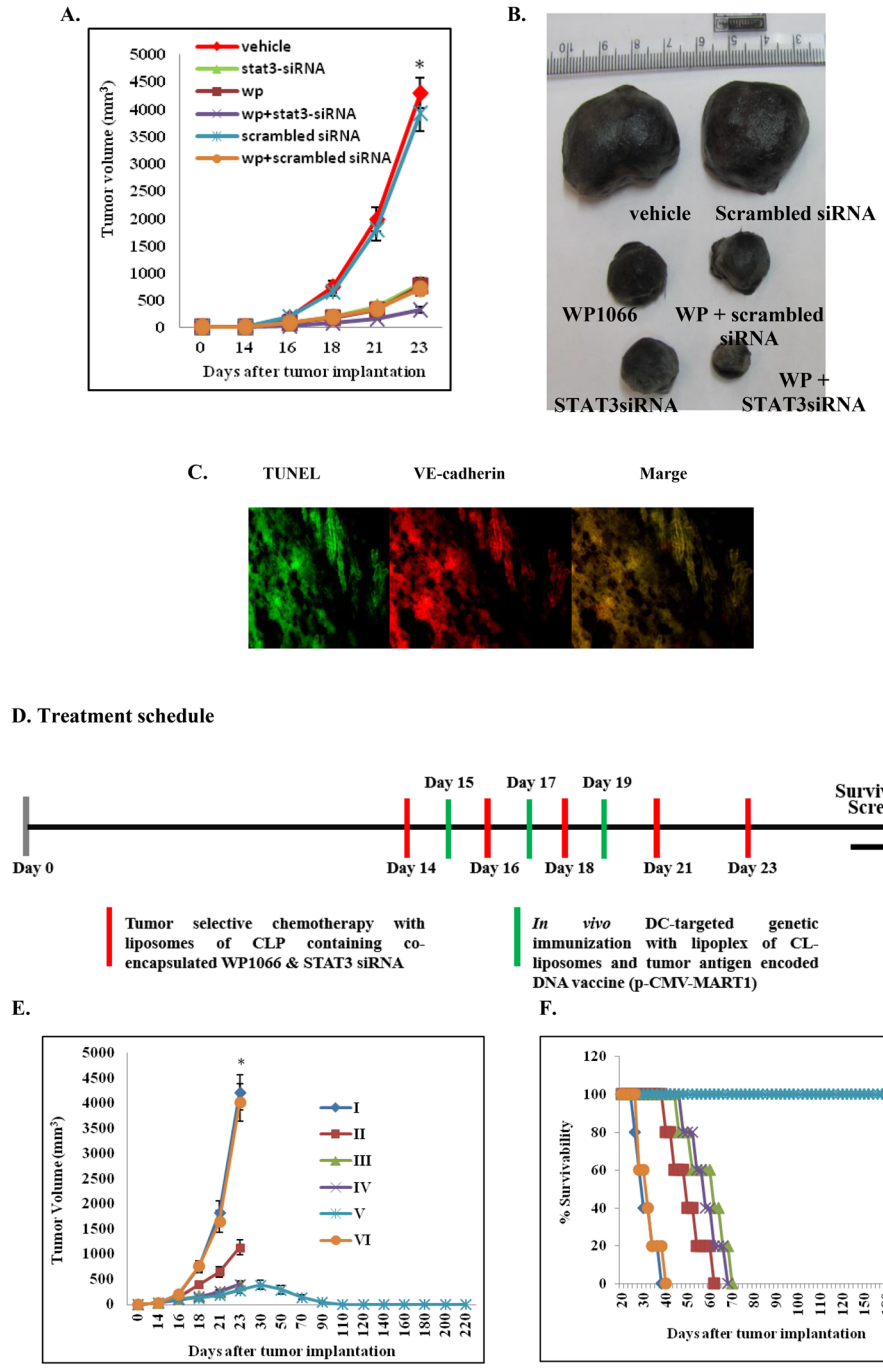

Fig. 4 Tumor selective chemotherapy with CLP-liposomes containing co-encapsulated WP1066 and STAT3 siRNA in combination with *in vivo* DC-targeted genetic immunization with lipoplexes of CL liposomes and a melanoma antigen (MART-1) encoded DNA vaccine results in the eradication of the established mouse melanoma. (A) Relative tumor growth inhibition in the mouse groups (n = 5) treated with CLP liposomes containing only WP1066, CLP liposomes containing only STAT3 siRNA, and CLP liposomes containing only scrambled siRNA; targeted liposomal formulation containing both WP1066 and scrambled siRNA; and targeted liposomal formulation containing both WP1066 and STAT3 siRNA. (B) Representative tumor sizes in each group on day 24 post tumor inoculation. (C) On day 24 post tumor inoculation, the fixed tumor cryosections from the mice treated with the targeted liposomal formulation containing both WP1066 and STAT3 siRNA were immunostained using an anti-VE-cadherin antibody (markers of tumor endothelial cells) and a TUNEL assay kit (markers for apoptotic cells, green). All the images were taken at ×10 magnification. (D) Treatment schedule. (E) Relative tumor growth inhibition observed in the mouse groups i.v. treated with only the vehicle control 5% glucose (I), only *in vivo* DC-targeting CL-liposomes in complexation with the melanoma antigen (MART-1) encoded DNA vaccine (Lipo-MART1, II), only (STAT3 siRNA and WP1066) co-loaded CLP liposomes (III), simultaneously with the control non-specific lipoplexes of the p-CMV-β-gal plasmid and *in vivo* DC-targeting CL liposomes and (WP1066 + STAT3 siRNA) co-loaded CLP liposomes ((Lipo-(WP + STAT3 siRNA) + Lipo-β-gal), IV), simultaneously with lipoplexes of the melanoma antigen (MART-1) encoded DNA vaccine (p-CMV-MART-1) and *in vivo* DC-targeting CL liposomes and (WP1066 + STAT3 siRNA) co-loaded CLP liposomes (Lipo-(WP + STAT3 siRNA) + Lipo-MART1, V), and empty CLP liposomes (VI). (F) Day 25 onwards, mice were subjected to a survival study. *P < 0.05 with respect to the tumor sizes for the 5% glucose treatment.

the cytokine secretion assays revealed remarkably higher amounts of IFN-γ and IL-4 secreted by the activated T cells in mice receiving the combined treatment (Fig. S14B and C, ESI‡). Thus, the findings summarized in Fig. S12A–C‡ indicate that heightened cellular immune responses may play crucial roles in the observed eradication of the established melanoma in mice receiving the presently described combination therapy.

The observed synergistic therapeutic outcome in the combination approach described herein presumably originates from enhanced DC maturation (and hence more T-cell mediated killing of tumor cells) resulting from the inhibition of STAT3 activation by WP1066-loaded liposomes of CLP. In other words, in the initial phases of the treatment schedules, the concentrations of immunosuppressive factors in the tumor microenvironment were likely to be at much higher concentrations than their concentrations at the end of the treatment schedules. Presumably, during the initial phase of the treatment schedule, immunosuppressive factors dominated the race between immunosuppression-related tumor growth *vs.* T-cell mediated tumor cell killing and the trend was reversed at the end of the treatment schedule. After the end of the treatment schedule, the pronounced decrease in the concentrations of the immunosuppressive factors in the tumor microenvironment might have significantly enhanced DC maturation, eventually leading to T-cell mediated eradication of the established mouse melanoma. Such a mechanistic possibility might play a key role in the observed slow increase of the tumor volume, followed by a gradual decrease of the tumor volume and eventual eradication of the established mouse melanoma in group V mice (Fig. 4E). Prior reports also showed that targeting small molecule inhibitors of the JAK/STAT pathway selectively to the tumor site is capable of inducing antitumor immune responses in the tumor microenvironment.[61,62] Besides cell-mediated immunity mounted by T-cells, natural killer (NK) cells are primary effectors of innate immunity against transformed tumor cells.[63,64] Bellucci *et al.* demonstrated increased susceptibility of tumor cells to NK cells upon treatment with tyrosine kinase inhibitors.[65] Such enhanced activities of NK cells may also play an important role in the presently observed synergistic therapeutic outcome. Clearly, in-depth mechanistic studies need to be carried out in future to decipher the origin of the observed synergy between tumor-selective chemotherapy and *in vivo* DC-targeted genetic immunization. Whether or not other potent commercially available JAK-STAT inhibitors (about 10 available)[46] would be equally efficient for use in our present combination approach needs to be studied in future. Similarly, whether the present combination approach works efficiently for other melanoma antigen encoded DNA vaccines[66] (*e.g.* DNA vaccines encoding melanoma antigens gp100, tyrosinase related protein1, *etc.*) needs to be examined in future. The preclinical findings described herein are expected to attract interest among the physician scientists for undertaking clinical studies aimed at exploring the therapeutic promise of the present combination approach in cancer patients.

Conclusions

We have shown that the use of tumor-selective chemotherapy in combination with *in vivo* dendritic cell (DC) targeted DNA vaccination eradicates established mouse melanoma. Liposomes of a newly synthesized lipopeptide containing a previously reported tumor-targeting CGKRK-ligand were used for tumor selective delivery of liposomally co-loaded cancer therapeutics STAT3siRNA and WP1066 (a commercially available inhibitor of the JAK2/STAT3 pathway). *In vivo* targeting of a melanoma antigen (MART-1) encoded DNA vaccine (p-CMV-MART1) to dendritic cells was accomplished by complexing it with a previously reported mannose-receptor selective *in vivo* DC-targeting cationic liposome. Liposomes of the CGKRK-lipopeptide containing encapsulated FITC-labeled siRNA, upon intravenous administration in B16F10 melanoma bearing mice, showed remarkably higher accumulation in tumors 24 h post i.v. treatment, compared to their degree of accumulation in other body tissues including the lungs, liver, kidneys, spleen and heart. Importantly, findings in tumor growth inhibition studies revealed that only *in vivo* DC-targeted genetic immunization or only tumor-selective chemotherapy using the presently described systems failed to eradicate the established mouse melanoma. Since the presently described combination therapy avoids the need for painstaking isolation of DCs or T-cells, and their *ex vivo* transduction and subsequent reinfusion into the recipient's body, this unique combination approach is expected to find future uses in combating established melanoma and possibly other solid tumors containing distinguishing tumor antigens.

Author contributions

A. C. and S. B. conceived this project and designed the experiments; S. B. and S. S. carried out the major work of the experimental parts reported in this manuscript; Y. V. and G. K. M. contributed in both *in vitro* and *in vivo* experiments and designed the experiments; and A. C. and S. B. wrote the manuscript with inputs from all the other authors.

Conflicts of interest

S. B., S. S. and A. C. are inventors of US Patent No. 9944676B2, issued on April 17, 2018.

Acknowledgements

A. C. thanks the Council of Scientific and Industrial Research (CSIR), Government of India for funding this work (project codes: CSC0302 and BSC0123) and the Indian Council of Medical Research (ICMR), Government of India, for awarding him an ICMR Emeritus Scientist position. S. B. and G. K. M. thank CSIR, Government of India, for their doctoral fellowships, Y. V. thanks the University Grant Commission (UGC),

Government of India, New Delhi, for his doctoral fellowship and S. S. thanks CSIR, Government of India for awarding him the Shyama Prasad Mukherjee Fellowship for pursuing doctoral research.

References

1 R. M. Steinman and Z. A. Cohn, *J. Exp. Med.*, 1973, **137**, 1142–1162.
2 G. J. Randolph, *J. Exp. Med.*, 2021, **218**, e20202077.
3 A. Harari, M. Graciotti, M. Bassani-Sternberg and L. E. Kandalaft, *Nat. Rev. Drug Discovery*, 2020, **19**, 635–652.
4 S. Nava, D. Lisini, S. Frigerio, S. Pogliani, S. Pellegatta, L. Gatti, G. Finocchiaro, A. Bersano and E. A. Parati, *Pharmaceutics*, 2020, **12**, 215–227.
5 S. Jhunjhunwala, C. Hammer and L. Delamarre, *Nat. Rev. Cancer*, 2021, **21**, 298–312.
6 S. C. Eisenbarth, *Nat. Rev. Immunol.*, 2019, **19**, 89–103.
7 O. P. Joffre, E. Segura, A. Savina and S. Amigorena, *Nat. Rev. Immunol.*, 2012, **12**, 557–569.
8 Y. Lu, Y. Shi and J. You, *J. Controlled Release*, 2022, **341**, 184–205.
9 M. Sadeghzadeh, S. Bornehdeli, H. Mohahammadrezakhani, M. Abolghasemi, E. Poursaei, M. Asadi, V. Zafari, L. Aghebati-Maleki and D. Shanehbandi, *Life Sci.*, 2020, **254**, 117580.
10 A. Gardner, A. P. de Mingo and B. Ruffell, *Front. Immunol.*, 2020, **11**, 924.
11 S. K. Wculek, F. J. Cueto, A. M. Mujal, I. Melero, M. F. Krummel and D. Sancho, *Nat. Rev. Immunol.*, 2020, **20**, 7–24.
12 G. Y-Z. X. Zhao and X.-R. Song, *Acta Pharmacol. Sin.*, 2020, **41**, 959–969.
13 P. Han, D. Hanlon, O. Sobolev, R. Chaudhury and R. L. Edelson, *Int. Rev. Cell Mol. Biol.*, 2019, **349**, 251–307.
14 B. Giri, P. Sharma, T. Jain, A. Ferrantella, U. Vaish, S. Mehra, B. Garg, S. Iyer, V. Sethi, Z. Malchiodi, *et al.*, *OncoImmunology*, 2021, **10**, 1976952.
15 C. I. DeVette, H. Gundlapalli, S.-C. A. Lai, C. P. McMurtrey, A. R. Hoover, H. R. Gurung, W. R. Chen, A. L. Welm and W. H. Hildebrand, *Oncoimmunology*, 2020, **9**, 1685300.
16 J. Rice, C. H. Ottensmeier and F. K. Stevenson, DNA vaccines: precision tools for activating effective immunity against cancer, *Nat. Rev. Cancer*, 2008, **8**, 108–120.
17 O. Akbari, N. Panjwani, S. Garcia, R. Tascon, D. Lowrie and B. Stockinger, *J. Exp. Med.*, 1999, **189**, 169–178.
18 J. Banchereau and R. M. Steinman, *Nature*, 1998, **392**, 245–252.
19 M. L. Hedley, J. Curley and R. Urban, *Nat. Med.*, 1998, **4**, 365–368.
20 M. Singh, M. Briones, G. Ott and D. O'Hagan, *Proc. Natl. Acad. Sci. U. S. A.*, 2000, **97**, 811–816.
21 A. S. Irvine, P. K. Trinder, D. L. Laughton, H. Ketteringham, R. H. McDermott, C. Reid, A. M. Haines, A. Amir, R. Husain, R. Doshi, L. L. S. Young and A. Mountain, *Nat. Biotechnol.*, 2000, **18**, 1273–1278.
22 Y. Hattori, S. Kawakami, S. Suzuki, F. Yamashita and M. Hashida, *Biochem. Biophys. Res. Commun.*, 2004, **317**, 992–999.
23 W. Wijagkanalan, S. Kawakami, M. Takenaga, R. Igarashi, F. Yamashita and M. Hashida, *J. Controlled Release*, 2008, **125**, 121–130.
24 Y. Lu, S. Kawakami, F. Yamashita and M. Hashida, *Biomaterials*, 2007, **28**, 3255–3262.
25 R. Srinivas, P. P. Karmali, D. Pramanik, A. Garu, Y. Mahidhar, B. K. Majeti, S. Ramakrishna, G. Srinivas and A. Chaudhuri, *J. Med. Chem.*, 2010, **53**, 1387–1391.
26 R. Srinivas, A. Garu, G. Moku, S. Agawane and A. Chaudhuri, *Biomaterials*, 2012, **33**, 6220–6229.
27 C. Voshavar, R. C. Meka, S. Samanta, S. Marepally and A. Chaudhuri, *J. Med. Chem.*, 2017, **60**, 1605–1610.
28 R. C. Reddy, S. Mukherjee, C. R. Patra and A. Chaudhuri, *Nanoscale*, 2019, **11**, 7931–7943.
29 A. Garu, G. Moku, S. K. Gulla and A. Chaudhuri, *Mol. Ther.*, 2016, **24**, 385–397.
30 S. K. Gulla, B. R. Rao, G. Moku, S. Jinka, N. V. Nimmu, S. Khalid, C. R. Patra and A. Chaudhuri, *Biomater. Sci.*, 2019, **7**, 773–788.
31 M. V. Gulijk, F. Dammeijer, J. G. J. V. Aerts and H. Vroman, *Front. Immunol.*, 2018, **9**, 2759.
32 G.-Y. Jang, Y. S. Kim, S. E. Lee, J. W. Lee, H. D. Han, T. H. Kang and Y.-M. Park, *Cancer Immunol., Immunother.*, 2021, **70**, 1075–1088.
33 S. P. Lau, N. van Montfoort, P. Kinderman, M. Lukkes, L. Klaase, M. van Nimwegen, M. van Gulijk, J. Dumas, D. Mustafa, S. L. A. Lievense, *et al.*, *J. Immunother. Cancer*, 2020, **8**, e000772.
34 T. Oba, K. Makino, R. Kajihara, T. Yokoi, R. Araki, M. Abe, H. Minderman, A. E. Chang, K. Odunsi and F. Ito, *J. Immunother. Cancer*, 2021, **9**, e002432.
35 J. Guo, E. Muse, A. J. Christians, S. J. Swanson and E. Davila, *Cancer Immunol. Res.*, 2019, **7**, 1523–1534.
36 M. Bassani-Sternberg, A. Digklia, F. Huber, D. Wagner, C. Sempoux, B. J. Stevenson, A.-C. Thierry, J. Michaux, H. Pak, J. Racle, *et al.*, *Front. Immunol.*, 2019, **10**, 1832.
37 R. Ramanathan, H. Choudry, H. Jones, M. Girgis, W. Gooding, P. Kalinski and D. L. Bartlett, *Ann. Surg. Oncol.*, 2021, **28**, 4637–4646.
38 S. Bhunia, V. Vangala, D. Bhattacharya, H. G. Ravuri, M. Kuncha, S. Chakravarty, S. Ramakrishna and A. Chaudhuri, *Mol. Pharm.*, 2017, **14**, 3834–3847.
39 S. Saha, V. Yakati, D. Bhattacharya, S. D. Kompella, M. Kuncha, S. Chakravarty, S. Ramakrishna and A. Chaudhuri, *Adv. Biosyst.*, 2017, **1**, 1600009.
40 J. A. Hoffman, E. Giraudo, M. Singh, L. Zhang, M. Inoue, K. Porkka, *et al.*, *Cancer Cell*, 2003, **4**, 383–391.
41 L. Agemy, D. Friedmann-Morvinski, V. R. Kotamraju, L. Roth, K. N. Sugahara, O. M. Girard, *et al.*, *Proc. Natl. Acad. Sci. U. S. A.*, 2011, **108**, 17450–17455.

42 X. L. Yao, Y. Yoshioka, G. X. Ruan, Y. Z. Chen, H. Mizuguchi, Y. Mukai, *et al.*, *Biomacromolecules*, 2012, **13**, 2402–2409.
43 Q. Hu, X. Gao, T. Kang, X. Feng, D. Jiang, Y. Tu, Q. Song, L. Yao, X. Jiang, H. Chen and J. Chen, *Biomaterials*, 2013, **34**, 9496–9508.
44 S. K. Gulla, R. Kotcherlakota, S. Nimushakavi, N. V. Nimmu, S. Khalid, C. R. Patra and A. Chaudhuri, *ACS Omega*, 2018, **3**, 8663–8676.
45 M. Tolomeo and A. Cascio, *Int. J. Mol. Sci.*, 2021, **22**, 603.
46 Z. Qureshy, D. E. Johnson and J. R. Grandis, *J. Cancer Metastasis Treat.*, 2020, **6**, 27.
47 R. Morris, N. J. Kershaw and J. J. Babon, *Protein Sci.*, 2018, **27**, 1984–2009.
48 J. S. Rawlings, K. M. Rosler and D. A. Harrison, *J. Cell Sci.*, 2004, **117**, 1281–1283.
49 C. P. Lim and X. Cao, *Mol. BioSyst.*, 2006, **2**, 536–550.
50 J. V. Alvarez, D. A. Frank, J. Alvarez and F. Lab, *Cancer Biol. Ther.*, 2004, **3**, 1045–1050.
51 W. Vainchenker and S. N. Constantinescu, *Oncogene*, 2013, **32**, 2601–2613.
52 Y. Wang, Y. Shen, S. Wang, Q. Shen and X. Zhou, *Cancer Lett.*, 2018, **415**, 117–128.
53 H. Yu, M. Kortylewski and D. Pardoll, *Nat. Rev. Immunol.*, 2007, **7**, 41–51.
54 H. Yu, D. Pardoll and R. Jove, *Nat. Rev. Cancer*, 2009, **9**, 798–809.
55 D. Gabrilovich, *Nat. Rev. Immunol.*, 2004, **4**, 941–952.
56 A. Ferrajoli, S. Faderl, Q. Van, P. Koch, D. Harris, *et al.*, *Cancer Res.*, 2007, **67**, 11291–11299.
57 A. Horiguchi, T. Asano, K. Kuroda, A. Sato, J. Asakuma, *et al.*, *Br. J. Cancer*, 2010, **102**, 1592–1599.
58 X. Zhou, Y. Ren, A. Liu, L. Han, K. Zhang, *et al.*, *Oncol. Rep.*, 2014, **31**, 2173–2180.
59 L. Kong, K. A. Mohamed, W. Jun, A. Chakraborty, *et al.*, *Clin. Cancer Res.*, 2008, **14**, 5759–5768.
60 V. Vangala, N. V. Nimmu, S. Khalid, M. Kuncha, R. Sistla, R. Banerjee and A. Chaudhuri, *Mol. Pharm.*, 2020, **17**, 1859–1874.
61 W. Zou, *Nat. Rev. Cancer*, 2005, **5**, 263–274.
62 T. Wang, G. Niu, M. Kortylewski, L. Burdelya, K. Shain, S. Zhang, R. Bhattacharya, D. Gabrilovich, R. Heller, D. Coppola, W. Dalton, R. Jove, D. Pardoll and H. Yu, *Nat. Med.*, 2004, **10**, 48–54.
63 M. A. Caligiu, *Blood*, 2008, **112**, 461–469.
64 E. Vivier, D. H. Raulet, A. Moretta, M. A. Caligiuri, L. Zitvogel, L. L. Lanier, W. M. Yokoyama and A. S. Ugolini, *Science*, 2011, **331**, 44–49.
65 R. Bellucci, H. N. Nguyen, A. Martin, S. Heinrichs, A. C. Schinzel, W. C. Hahn and J. Ritz, *J. Clin. Invest.*, 2012, **122**, 2369–2383.
66 T. Rezaei, E. Davoudian, S. Khalili, A. M. Amini, M. Hejazi, *et al.*, *Pigm. Cell Melanoma Res.*, 2021, **34**, 869–891.

